Journal of Alloys and Compounds 513 (2012) 399–403

Contents lists available at SciVerse ScienceDirect

Journal of Alloys and Compounds

journal homepage: www.elsevier.com/locate/jallcom

MgZnO/MgO strained multiple-quantum-well nanocolumnar films: Stress-induced structural transition and deep ultraviolet emission

L. Wang[a,b], H.Y. Xu[a,*], C. Zhang[a], X.H. Li[a], Y.C. Liu[a,*], X.T. Zhang[a], Y. Tao[c], Y. Huang[c], D.L. Chen[c]

[a] Centre for Advanced Optoelectronic Functional Materials Research and Key Laboratory for UV Light-Emitting Materials and Technology of Ministry of Education, Northeast Normal University, Changchun 130024, PR China
[b] Department of Applied Physics, College of Sciences, Nanjing University of Technology, Nanjing 210009, PR China
[c] Beijing Synchrotron Radiation Facility, Institute of High Energy Physics, Chinese Academy of Science, Beijing 100049, PR China

ARTICLE INFO

Article history:
Received 10 August 2011
Received in revised form 13 October 2011
Accepted 15 October 2011
Available online 25 October 2011

Keywords:
MgZnO/MgO
Multiple-quantum-well
Nanocolumn
Structural transition
Deep ultraviolet

ABSTRACT

MgZnO/MgO strained multiple-quantum-wells (S-MQWs) with different structures are grown by pulsed laser deposition. The S-MQW films are composed of closely arranged, vertically oriented nanocolumns. Z-contrast scanning transmission electron microscopy observations and line-scan compositional analysis reveal that the nanocolumns are compositionally modulated along their length and have a MQW structure. A coherent epitaxial relationship with a sharp interface is established between MgZnO and MgO layers with large lattice mismatch. It is worth noting that the MgZnO layer undergoes a structural transition from hexagonal to cubic phase with its thickness decreasing. The calculations reveal that a large in-plane compressive stress dominates such an interesting phase transition process, stabilizes the low Mg-content MgZnO alloy in the anomalous cubic phase, and also leads to a broadening of the band gap. As a result, the wavelength-tunable deep-ultraviolet emission in the range of 261–314 nm is obtained from these S-MQW nanocolumnar films. The 261 nm is known to be the shortest emission wavelength ever reported for MgZnO material.

1. Introduction

Deep-ultraviolet (DUV) light emitting devices are attracting growing interest due to their many potential applications in high-density optical data storage, microelectronic fabrication technology, environmental protection, bio-medicine, etc. MgZnO ternary alloy has continuously tunable band gaps from 3.37 to 7.70 eV in theory, large exciton binding energy and relatively low growth temperature. These make it a promising material for developing the DUV light-emitting diodes (LEDs) and laser diodes (LDs). Most previous studies focus on using MgZnO as a potential barrier material for ZnO/MgZnO quantum wells (QWs) [1–4]. Such a QW structure is widely used in the LED/LD devices to increase their radiative recombination efficiency. In order to further shorten the emission wavelength into the DUV region, the MgZnO film should serve as the active layer; in this case, the wide band gap MgO can be chosen as a possible barrier material to construct MgZnO/MgO QWs. The large energy-band offset between them will make the carrier confinement stronger than that in the conventional ZnO/MgZnO QWs. However, it is known that MgZnO usually stabilizes in a wurtzite structure (hexagonal symmetry) when the Mg content is below 33 at.% [5–7], while MgO has a rock-salt structure (cubic symmetry). Their structural difference and lattice mismatch will lead to a large strain and a high density of defects in QW films. Thus, almost no report is available on such a novel QW structure. Studies on the growth of GaN-based materials have proved that column crystal growth is an effective way to relax part of the stress and improve the quality of the epitaxial layers [8–11]. Highly efficient LEDs have also been fabricated from nanocolumnar GaN-based crystals [12–14]. The formation of one-dimensional (1D) nanocolumnar microstructure allows the combination of materials with large lattice mismatch without generating dislocations. On the other hand, energy band engineering and strain engineering can also be realized in such 1D heterostructures, giving rise to some novel low-dimensional physical phenomena. In this work, we have designed and grown the MgZnO/MgO strained multiple-quantum-well (S-MQW) nanocolumnar films with different structures, and observed that the MgZnO layer underwent a stress-induced structural transition from hexagonal to cubic phase with its thickness decreasing. The wavelength-tunable DUV emission in the range of 261–314 nm is obtained from these S-MQW nanocolumnar films. To the best of our knowledge, the 261 nm is the shortest emission wavelength ever reported for MgZnO material.

2. Experimental details

The MgZnO/MgO S-MQW nanocolumnar films were grown on the c-plane Al_2O_3 substrates by pulsed laser deposition (PLD). Prior

* Corresponding authors. Tel.: +86 431 85099168; fax: +86 431 85684009.
E-mail addresses: hyxu@nenu.edu.cn (H.Y. Xu), ycliu@nenu.edu.cn (Y.C. Liu).

0925-8388/$ – see front matter © 2011 Elsevier B.V. All rights reserved.
doi:10.1016/j.jallcom.2011.10.056

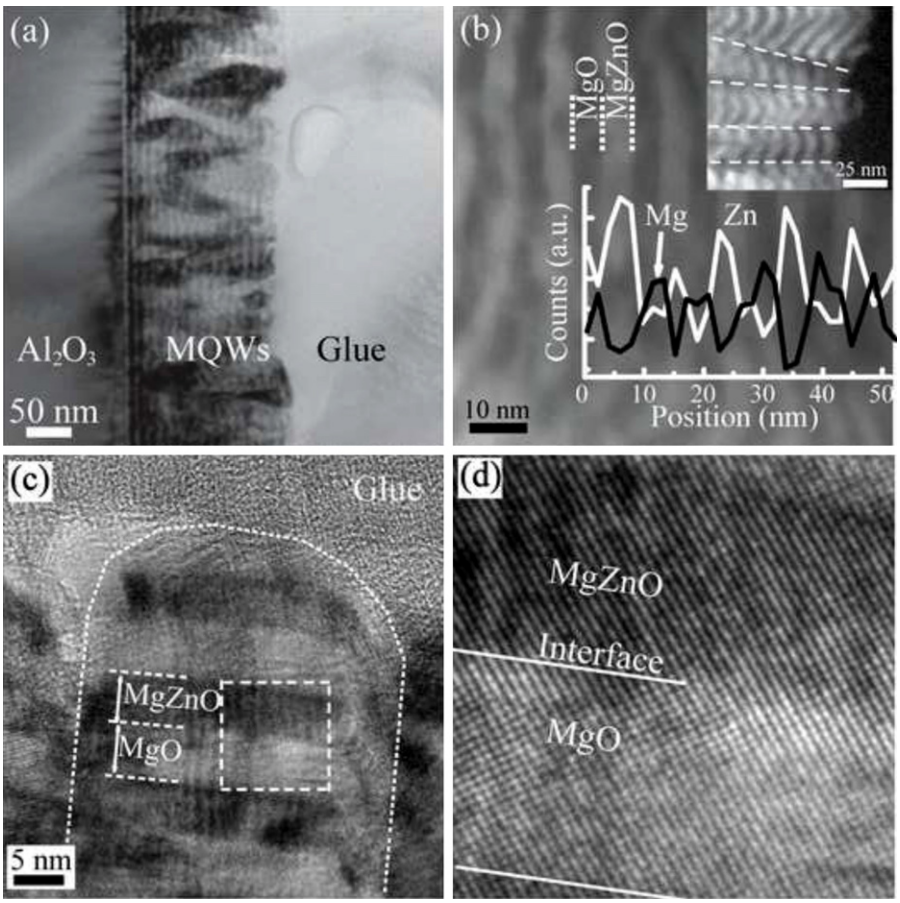

Fig. 1. Cross-sectional TEM images of an MgZnO/MgO S-MQW nanocolumnar film with MgZnO layer thickness of ~5 nm (sample 2). (a) A large-scale bright field image of the cross section of the sample 2. (b) A magnified HAADF-STEM image taken on a single nanocolumn. The dark and light regions correspond to the MgO and MgZnO layers, respectively. Top inset: a Z-contrast STEM image, which reveal that the sample consists of closely arranged nanocolumns. Bottom inset: the line-scan composition profiles of Zn and Mg elements along the nanocolumn's length. (c) High resolution TEM image of an individual nanocolumn. (d) Lattice-resolved image of the rectangular region marked in (c).

to deposition, the growth chamber was evacuated to a base pressure below 5×10^{-5} Pa with a turbo molecular pump, and the Al_2O_3 substrates were in situ thermally cleaned at 800 °C for 30 min at this vacuum level. Then, ultrapure O_2 gas was introduced into the chamber. Throughout the entire growth process, the O_2 pressure and substrate temperature were kept at 20 Pa and 400 °C, respectively. A Nd:YAG pulsed laser (λ = 355 nm, ts = 5 ns, repetition rate = 10 Hz, power density = 7.6×10^8 W/cm^2) was employed to ablate MgO and MgZnO targets alternately to realize the MQW growth. All the MQW nanocolumnar films consist of 16 unit layers, and each unit layer is composed of MgZnO and MgO sublayers. Our experimental design is that the total laser pulse count is kept constant at 4500 for the growth of each unit layer, but the ratio of the pulse count used to grow MgZnO and MgO sublayers is variable, and set at 2, 0.5 and 0.25 for the samples 1, 2 and 3, respectively. Considering the growth rates of MgZnO (0.033 Å/pulse) and MgO (0.020 Å/pulse), the resulting MgZnO/MgO sublayer thickness is estimated to be 10/3 nm, 5/6 nm and 3/7.2 nm for three samples. Moreover, as the reference sample, two thick MgZnO films were also deposited on the Al_2O_3 substrates with and without an MgO buffer layer at the same conditions.

3. Results and discussion

The structure of the samples is examined by the cross-sectional transmission electron microscopy (TEM). Fig. 1 displays the TEM images of sample 2. In the bright field image in Fig. 1a, alternating light/dark stripes parallel to the substrate surface are clearly seen, suggesting the formation of MQW structure. A closer look reveals that the film is not continuous but textured, that is, the film is composed of closely arranged nanocolumns. The orientation of the nanocolumns tends to be perpendicular to the substrate surface, and their diameter and height are about 25 nm and 175 nm. The nanocolumn consists of 16 MgZnO/MgO unit layers. Such a MQW structure can be further confirmed by a more obvious contrast in a high-angle annular dark field scanning TEM (HAADF-STEM) image, which is sensitive to the atomic number of elements. In Fig. 1b, the dark and light regions correspond to the MgO and MgZnO sublayers, respectively, because the former containing lighter element is a relatively weak electron scatterer. We have also observed a periodic spatial modulation of composition by line-scan energy dispersive X-ray (EDX) microanalysis. As shown in the bottom inset of Fig. 1b, the Zn signal fluctuates periodically along the nanocolumn's length, while the Mg signal exhibits an opposite variation trend. The signal period is roughly equal to the thickness of the unit layer, suggesting that no obvious inter-diffusion of atoms occurs. Fig. 1c and d are lattice-resolved TEM images of an individual nanocolumn. The near-perfect lattice fringes confirm that both MgZnO and MgO layers are single-crystalline, and few dislocations and stacking faults were observed even in their interfacial region. A coherent epitaxial relationship with a sharp interface has been established between MgZnO and MgO layers with large lattice mismatch. Thus, it is conceivable that both layers suffer from high in-plane stress.

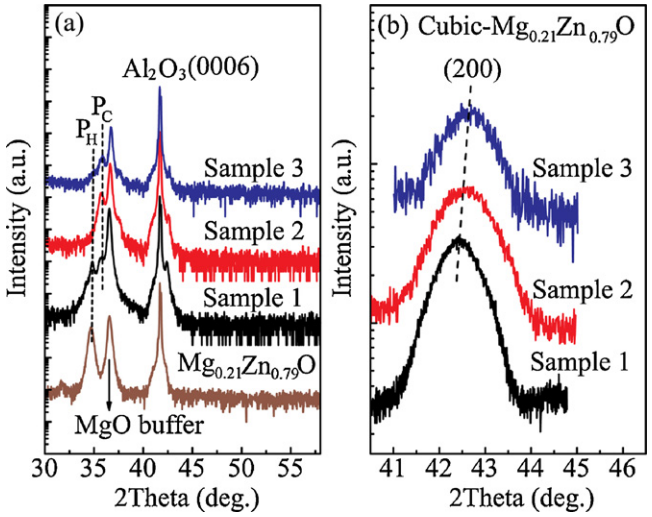

Fig. 2. (a) The normal $\omega/2\theta$ scan XRD patterns of MgZnO/MgO S-MQWs and a thick MgZnO film on MgO buffer layer. (b) The off-normal XRD $\omega/2\theta$ scans of the cubic MgZnO (2 0 0) reflection in the 2θ range of 40–45°. Both *y*-axes are plotted in logarithmic scale.

To get more detailed information on the crystal structure, epitaxial relationship and lattice constant of the samples, the X-ray diffraction (XRD) scans were performed along normal and off-normal directions of the sample surface by means of a Rigaku Dmax/2500 (40 kV/100 mA, scan rate 5°/min) and a Bruker D8-advance (40 kV/40 mA, scan rate 3°/min) XRD meter with Cu Kα line (1.5406 Å), respectively. Fig. 2a shows the normal $\omega/2\theta$ scan data. The diffraction peaks at 36.55° and 41.68°, present in all the XRD patterns, correspond to the (1 1 1) reflection of cubic MgO and the (0 0 0 6) reflection of Al_2O_3 substrate, respectively. For the MgZnO film, besides these two peaks, only (0 0 0 2) diffraction peak of the wurtzite structure (P_H) is detected, indicating that the MgZnO film grown on MgO buffer layer crystallizes in a usual *c*-axis oriented hexagonal phase. It is interesting to note that a new peak centered at 35.69° (P_C) appears in the XRD pattern of the sample 1, which can be indexed to the (1 1 1) reflection of cubic MgZnO. As the MgZnO layer thickness gradually decreases from 10 to 3 nm, the P_H rapidly decays in intensity and completely disappears, while the P_C becomes more evident. The change in the relative intensity of P_C to P_H reflects a hexagonal-to-cubic structural transition of MgZnO layer with its thickness decreasing. Similar to this observation, several groups have also found that when the ZnO or MgZnO film is epitaxially grown on the MgO (1 1 1) buffer layer, a cubic-phase ultrathin layer can form at the initial stage of the growth [15–17]. However, the formation mechanism of anomalous cubic phase is not fully understood. It is known that a phase transition from hexagonal to cubic MgZnO usually occurs when the Mg content exceeds ~60 at.%. Though the inter-diffusion may lead to an increase of Mg content in MgZnO layers, this possibility has been ruled out by the results of Z-contrast STEM and compositional line scan, which determine the Mg content of MgZnO layers to be only 21 at.% in our MQW structures. Further, Ohtomo et al. [18] have observed that Mg atoms start to inter-diffuse only above 700 °C, and our growth temperature of 400 °C is far lower than this critical temperature. On the other hand, the lattice constant of MgZnO is larger than that of MgO; when a coherent epitaxial relationship is established between them, a compressive stress will be applied to the MgZnO layer. It has been reported in our previous studies that a high hydrostatic pressure can induce a transition of ZnO from hexagonal to cubic phase [19]. Thus, we deduce that the in-plane compressive stress is responsible for the formation of anomalous cubic MgZnO. The following calculations will support our point of view.

The off-normal XRD φ-scans of cubic MQWs show typical six-fold symmetric patterns (not shown here), suggesting an in-plane epitaxial relationship of $[1\,0\,\bar{1}]$ MgZnO//$[1\,0\,\bar{1}]$ MgO. In order to calculate the stress, the $[1\,0\,\bar{1}]$ interplanar spacing of cubic MgZnO ($d_{(1\,0\,\bar{1})}$) has to be known. Thus, we carried out XRD $\omega/2\theta$ scans of the cubic MgZnO (2 0 0) reflection by tilting the samples 54.7° around χ-axis, and the results are shown in Fig. 2b. It is found that as the MgZnO layer thickness decreases, its (2 0 0) diffraction peaks shift gradually toward higher angles, indicating a decrease in the lattice constant and an increase in the compressive stress. The in-plane stress can result in a lattice distortion and a slight deviation from the ideal cubic structure. Thus, the following equation, which is applicable to a rhombohedral lattice system [20], is used to calculate the interplanar spacing ($d_{(hkl)}$), where a and α are the lattice constant and axial angle, respectively.

$$\frac{1}{d^2_{(h\,k\,l)}} = \frac{(h^2+k^2+l^2)\sin^2\alpha + 2(hk+kl+hl)(\cos^2\alpha - \cos\alpha)}{a^2(1-3\cos^2\alpha+2\cos^3\alpha)} \quad (1)$$

Using the known values of $d_{(1\,1\,1)}$ and $d_{(2\,0\,0)}$, the a, α, and $d_{(1\,0\,\bar{1})}$ are calculated and listed in Table 1. The $[1\,0\,\bar{1}]$ interplanar spacing of stress-free cubic $Mg_{0.21}Zn_{0.79}O$ ($d'_{(1\,0\,\bar{1})}$) are determined as 3.185 Å from the virtual crystal approximation (VCA) [21–25], and the angle α is 90° for an ideal cubic structure. Obviously, the $d_{(1\,0\,\bar{1})}$ and α of our MQW structures are smaller than these theoretical values, confirming the presence of in-plane compressive stress. Further, the in-plane stress (σ) can be quantitatively determined by the equation below [26].

$$\sigma = -\frac{Y}{\nu}\frac{d_{(1\,0\,\bar{1})} - d'_{(1\,0\,\bar{1})}}{d'_{(1\,0\,\bar{1})}} \quad (2)$$

Here Y and ν are Young's modulus and Poisson's ratio, and their values are 155.9 GPa and 0.316 [22,27,28], respectively, for cubic $Mg_{0.21}Zn_{0.79}O$. The calculations yield σ = 31.7–34.0 GPa, which are far larger than the critical pressure of the phase transition of ZnO (8.3–9.5 GPa) [19,29,30]. Thus, the formation of anomalous cubic MgZnO may result from the large compressive stress. We also note that the stress σ slightly reduces from 34.0 to 31.7 GPa with increasing MgZnO layer thickness. This phenomenon can be understood by considering the stress relaxation. That is, as the MgZnO thickness increases, the stress is gradually relaxed by the introduction of defects. When the MgZnO layer exceeds a certain thickness [31], the stress will be below the phase transition pressure, the growth of cubic MgZnO cannot be maintained, and a structural transition to hexagonal phase takes place.

The optical absorption spectra of the S-MQW structures, pure $Mg_{0.21}Zn_{0.79}O$ and MgO films, were measured to determine their band gaps. As shown in Fig. 3, for the MgO film, no absorption edge

Table 1
The experimental and calculated results of structural parameters (a, α, $d_{(1\,0\,\bar{1})}$), stress (σ), stress-induced energy shift (ΔE_{stress}) and band gap shift (ΔE_g) for the MgZnO layers in S-MQW nanocolumnar films.

Sample	a (Å)	α (°)	$d_{(1\,0\,\bar{1})}$(Å)	σ (GPa)	ΔE_g (meV)	ΔE_{stress} (meV)
1	4.261	88.74	2.980	31.7	954	859
2	4.249	88.60	2.967	33.7	1079	913
3	4.244	88.66	2.965	34.0	1135	921

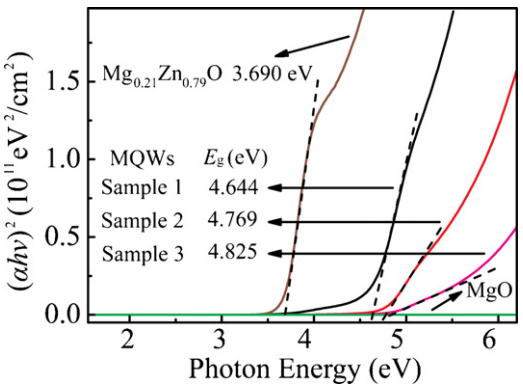

Fig. 3. Optical absorption spectra of all the samples measured at room temperature.

is observed in the measured range of 1.5–6.2 eV because of its wide band gap of ~7.70 eV. All the samples show high transmittance above 90% over the entire visible region. The absorption coefficient of the $Mg_{0.21}Zn_{0.79}O$ film increases rapidly above 3.4 eV, while the absorption edges of the S-MQW nanocolumnar films extend into the DUV region, and gradually shift toward shorter wavelengths with decreasing MgZnO layer thickness. By extrapolating the linear portion to $(\alpha h\nu)^2 = 0$ in the plot of $(\alpha h\nu)^2$ *vs.* $h\nu$ (α and $h\nu$ being absorption coefficient and photon energy), the band gap energy (E_g) is estimated to be 4.825, 4.769, 4.644 and 3.690 eV, respectively, for three different S-MQW samples and the $Mg_{0.21}Zn_{0.79}O$ film. The E_g of the MgZnO layers in S-MQW structures is blue-shifted by 1135 (sample 3), 1079 (sample 2) and 954 meV (sample 1) compared to that of the pure $Mg_{0.21}Zn_{0.79}O$ film. It is easy to think that such a relative energy shift (ΔE_g) may be associated with the quantum confinement effect (QCE). The QCE-induced energy shift (ΔE_{QCE}) increases with decreasing size and dimensionality. Even if in a 0D spherical nanocrystal system with a diameter equal to the MgZnO layer thickness, the calculated ΔE_{QCE} using the equations in Ref. [32] is no more than 122 meV, which is less than 11% of the total ΔE_g. In our case of 2D QWs, the ΔE_{QCE} will further reduce and only has a very small contribution to the observed ΔE_g. Thus, some other factors have to be considered. It is known that the compressive stress can induce not only a structural transition, but also a broadening of the band gap. The energy shift (ΔE_{stress}) is usually proportional to the stress (σ), namely, $\Delta E_{stress} = \beta\sigma$ [19], where β is a pressure coefficient (27.1 meV/GPa) [33]. Using this linear relationship, the ΔE_{stress} is calculated to be 921 (sample 3), 913 (sample 2) and 859 meV (sample 1), which account for at least 80% of the total ΔE_g. From the above calculations, we can conclude that the compressive stress dominates the band gap shift of MgZnO layers in S-MQWs into the DUV region.

Studies on the absorption spectra predict a possibility of obtaining DUV emission from these S-MQW nanocolumnar films. Fig. 4a exhibits the room-temperature photoluminescence (PL) spectra of all the samples. With the excitation of 325 nm line of a He–Cd laser, the pure $Mg_{0.21}Zn_{0.79}O$ film shows a near-band-edge (NBE) UV emission centered at 353 nm and a weak deep-level (DL) visible emission. The high energy side of the UV PL peak is partially cut off by the filter used to block the laser light. Since the photon energy of 325 nm laser is too low to excite the NBE emission of S-MQW samples, a 160 nm vacuum UV (VUV) light, which is emitted from 4B8 beamline at Beijing Synchrotron Radiation Facility, is used as the excitation source. As expected, the DUV emissions are achieved in these S-MQWs. With decreasing MgZnO layer thickness, their NBE PL peak shifts from 314 to 261 nm, and the emission wavelength is much shorter than that of the pure $Mg_{0.21}Zn_{0.79}O$ film (353 nm). The peak at ~230 nm observed in all the three samples comes from the indeterminate background, since it also appears in the VUV-excited

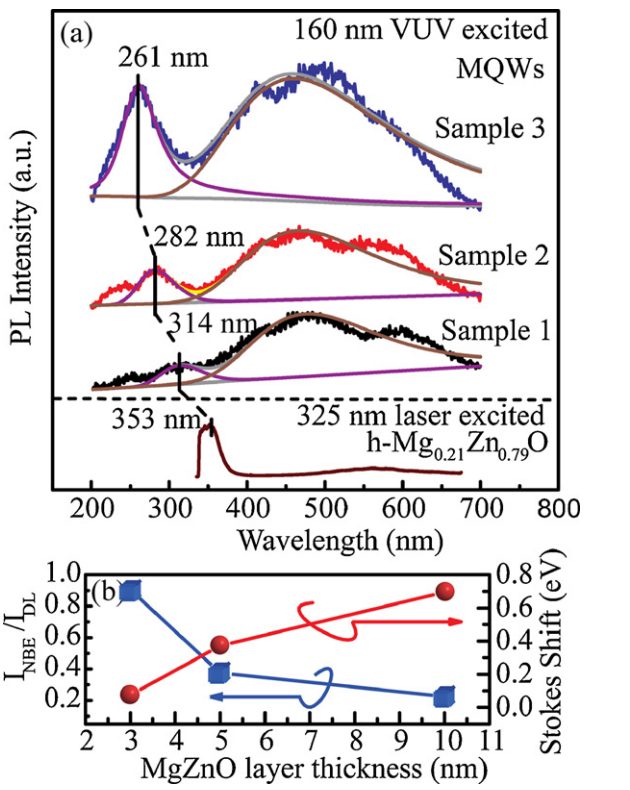

Fig. 4. (a) The room-temperature PL spectra of MgZnO/MgO S-MQWs and pure $Mg_{0.21}Zn_{0.79}O$ film, which were excited by 160 and 325 nm light sources, respectively. The solid lines are the Gaussian fits to the UV and visible emission bands. (b) The variations of I_{NBE}/I_{DL} (blue-cube dots) and Stokes shift (red-sphere dots) with the MgZnO layer thickness. (For interpretation of the references to color in this figure legend, the reader is referred to the web version of the article.)

PL spectrum of bare Al_2O_3 substrate (not shown here). Similar to the results of absorption spectra, the PL peak shift is mainly attributed to the compressive stress. The intensity ratio of NBE to DL emission (I_{NBE}/I_{DL}), as well as the Stokes shift (which is defined as the energy difference between the band gap and the PL peak), can be used to evaluate the crystal quality of MgZnO layer. In Fig. 4b, as the MgZnO thickness decreases, the ratio I_{NBE}/I_{DL} increases and the Stokes shift decreases. Such a variation trend suggests an improvement of the crystal quality of MgZnO layers. This is due to the reduction of defects accompanied by the stress relaxation process, as discussed above.

4. Conclusions

In conclusion, we have grown the MgZnO/MgO S-MQW nanocolumnar films by PLD technique, and studied their microstructural and optical properties. The nanocolumns are of MQW structure and compositionally modulated along their axial direction. Though the crystal structure and lattice constant of MgZnO and MgO are mismatched, the epitaxial growth with high-quality interface has been achieved between them. Herein, the good strain accommodation of nanocolumn heterostructures may play an important role. The large in-plane compressive stress (1) induces a structural transition of the MgZnO layer from hexagonal to cubic phase; (2) leads to a broadening of MgZnO band gap, and allows us to obtain a DUV emission with a wavelength as short as 261 nm. Thereby, it is possible that such a novel MgZnO/MgO QW structure, as an active layer, will be applied to DUV optoelectronic devices in the future.

Acknowledgments

This work was supported by National Natural Science Foundation of China (Grant No. 50725205, 51172041 and 60907016), Fund from Jilin Province (Grant No. 20100339, 20080102, FH0009), Cultivation Fund of NENU (Grant No. NENU-STC08001), and the Fundamental Research Funds for the Central Universities (No. 09SSXT118).

References

[1] W.I. Park, G.C. Yi, M. Kim, S.J. Pennycook, Adv. Mater. 15 (2003) 526.
[2] A. Ashrafi, J. Appl. Phys. 107 (2010) 123527.
[3] S. Chu, J.Z. Zhao, Z. Zheng, J.Y. Kong, L. Li, J.L. Liu, J. Appl. Phys. 109 (2011) 123110.
[4] X.Q. Lv, J.Y. Zhang, W.J. Liu, X.L. Hu, M. Chen, B.P. Zhang, J. Phys. D: Appl. Phys. 44 (2011) 365401.
[5] A. Ohtomo, M. Kawasaki, T. Koida, K. Masubuchi, H. Koinuma, Y. Sakurai, Y. Yoshida, T. Yasuda, Y. Segawa, Appl. Phys. Lett. 72 (1998) 2466.
[6] L.Q. Zhang, Z.Z. Ye, J.Y. Huang, B. Lu, H.P. He, J.G. Lu, Y.Z. Zhang, J. Jiang, J. Zhang, K.W. Wu, W.G. Zhang, J. Alloys Compd. 509 (2011) 7405.
[7] N. Panwar, J. Liriano, R.S. Katiyar, J. Alloys Compd. 509 (2011) 1222.
[8] H.W. Seo, Q.Y. Chen, M.N. Iliev, L.W. Tu, C.L. Hsiao, J.K. Mean, W.K. Chu, Appl. Phys. Lett. 88 (2006) 153124.
[9] A. Kikuchi, K. Yamano, M. Tada, K. Kishino, Phys. Status Solidi B 241 (2004) 2754.
[10] E. Calleja, M.A. Sánchez-García, F.J. Sánchez, F. Calle, F.B. Naranjo, E. Muñoz, U. Jahn, K. Ploog, Phys. Rev. B 62 (2000) 16826.
[11] N. Thillosen, K. Sebald, H. Hardtdegen, R. Meijers, R. Calarco, S. Montanari, N. Kaluza, J. Gutowski, H. Luth, Nano Lett. 6 (2006) 704.
[12] H.M. Kim, Y.H. Cho, H. Lee, S.I. Kim, S.R. Ryu, D.Y. Kim, T.W. Kang, K.S. Chung, Nano Lett. 4 (2004) 1059.
[13] A. Kikuchi, M. Kawai, M. Tada, K. Kishino, Jpn. J. Appl. Phys. 43 (2004) L1524.
[14] C.H. Chiu, P.M. Tu, C.C. Lin, D.W. Lin, Z.Y. Li, K.L. Chuang, J.R. Chang, T.C. Lu, H.W. Zan, C.Y. Chen, H.C. Kuo, S.C. Wang, C.Y. Chang, IEEE J. Sel. Top. Quant. Electron. 17 (2011) 971.
[15] Z. Vashaei, T. Minegishi, H. Suzuki, T. Hanada, M.W. Cho, T. Yao, A. Setiawan, J. Appl. Phys. 98 (2005) 054911.
[16] P. Bhattacharya, R.R. Das, R.S. Katiyar, Appl. Phys. Lett. 83 (2003) 2010.
[17] A. Kaushal, D. Kaur, J. Alloys Compd. 509 (2011) 200.
[18] A. Ohtomo, R. Shiroki, I. Ohkubo, H. Koinuma, M. Kawasaki, Appl. Phys. Lett. 75 (1999) 4088.
[19] S.J. Chen, Y.C. Liu, C.L. Shao, C.S. Xu, Y.X. Liu, C.Y. Liu, B.P. Zhang, L. Wang, B.B. Liu, G.T. Zou, Appl. Phys. Lett. 88 (2006) 133127, and the references therein.
[20] M.K. Miller, Atom Probe Tomography: Analysis at the Atomic Level, Springer, New York, 2000.
[21] L. Nordheim, Ann. Phys. 9 (1931) 607.
[22] The values of $d'_{(1\,0\,\bar{1})}$, Y, and ν for stress-free c-$Mg_{0.21}Zn_{0.79}O$ were estimated by VCA: $d'_{(\text{c-Mg}_x\text{Zn}_{1-x}\text{O})} = xd'_{\text{c-MgO}} + (1-x)d'_{\text{c-ZnO}}$. The lattice constants of c-ZnO (4.580 Å) and MgO (4.211 Å) are from: Refs. [23,24]. The $Y_{\text{c-ZnO}} = 119.0$ GPa, $\nu_{\text{c-ZnO}} = 0.351$, $Y_{\text{MgO}} = 294.7$ GPa and $\nu_{\text{MgO}} = 0.186$ are from Refs. [27,28].
[23] Data from the Website of Siliconfareast, http://www.siliconfareast.com/lattice_constants.htm.
[24] D. Fritsch, H. Schmidt, M. Grundmann, Appl. Phys. Lett. 88 (2006) 134104.
[25] K. Benkabou, N. Amrane, M. Maachou, J. Alloys Compd. 465 (2008) 305.
[26] R.W. Hoffman, in: C.H.S. Dupy, C. Cachard (Eds.), Physics of Nonmetallic Thin Films, Plenum, New York, 1976, p. 273.
[27] L.P. Martin, D. Dadon, M. Rosen, J. Am. Ceram. Soc. 79 (1996) 1281.
[28] S.M. Lang, Properties of High-temperature Ceramics and Cermets, Elasticity and Density at Room Temperature, Monograph 6, National Bureau of Standards, Washington, D.C., 1960.
[29] A. Segura, J.A. Sans, F.J. Manjón, A. Muñoz, M.J. Herrera-Cabrera, Appl. Phys. Lett. 83 (2003) 278.
[30] S.X. Cui, W.X. Feng, H.Q. Hu, Z.B. Feng, Y.X. Wang, J. Alloys Compd. 476 (2009) 306.
[31] K.W. Schwarz, Y. Tu, J. Appl. Phys. 106 (2009) 083510.
[32] L.E. Brus, J. Chem. Phys. 80 (1984) 4403.
[33] J. Huso, J.L. Morrison, H. Hoeck, X.B. Chen, L. Bergman, S.J. Jokela, M.D. McCluskey, T. Zheleva, Appl. Phys. Lett. 89 (2006) 171909.